HHS Public Access

Author manuscript

J Magn Reson Imaging. Author manuscript; available in PMC 2016 October 01.

Published in final edited form as:

J Magn Reson Imaging. 2015 October ; 42(4): 936–945. doi:10.1002/jmri.24871.

Dynamic Contrast Enhanced Magnetic Resonance Imaging Evaluates the Early Response of Human Head and Neck Tumor Xenografts following Anti-EMMPRIN therapy with Cisplatin or Irradiation

Hyunki Kim, PhD, MBA[1,5,6], **Yolanda E. Hartman, MS**[2], **Guihua Zhai, PhD**[1], **Thomas K. Chung, MD**[2], **Melissa L. Korb, MD**[2], **Timothy M. Beasley**[3], **Tong Zhou, MD**[4], and **Eben L. Rosenthal, MD**[2,5]

[1]Department of Radiology, University of Alabama at Birmingham, Birmingham, Alabama 35294-0019

[2]Department of Surgery, University of Alabama at Birmingham, Birmingham, Alabama 35294-0019

[3]Department of Biostatistics, University of Alabama at Birmingham, Birmingham, Alabama 35294-0019

[4]Department of Medicine, University of Alabama at Birmingham, Birmingham, Alabama 35294-0019

[5]Comprehensive Cancer Center, University of Alabama at Birmingham, Birmingham, Alabama 35294-0019

Abstract

Purpose—To assess the early therapeutic effects of anti-EMMPRIN antibody with/without cisplatin or X-ray radiation in head and neck cancer mouse models using dynamic contrast enhanced magnetic resonance imaging (DCE-MRI).

Materials and Methods—Mice bearing SCC1 (or OSC19) tumor xenografts were treated with anti-EMMPRIN antibody, radiation, cisplatin, or anti-EMMPRIN antibody plus cisplatin (or radiation) for a week (n=4–5 per group). DCE-MRI was carried out on a 9.4T small animal MR scanner on days 0, 3, and 7, and K^{trans} values were averaged in 0.5-mm thick peripheral tumor region. Ki67 and CD31 staining were implemented for all tumors after imaging.

Results—The K^{trans} changes of SCC1 and OSC19 tumors treated with anti-EMMPRIN antibody for 3 days were −18±8% and 4±7%, respectively, which were significantly lower than those of control groups (39±5% and 45±7%; p=0.0025 and 0.0220, respectively). When cisplatin was added, those were −42±9% and −44±9%, respectively, and with radiation, −45±9% and −27±10%, respectively, which were also significantly lower than those of control groups (p<0.0001 for all four comparisons). In the eight groups untreated (served as control) or treated with anti-

[6]Communicating author, and to whom requests for reprints should be addressed at G802C5 Volker Hall, 1670 University Blvd., Birmingham, AL 35294-0019. (phone: 205-996-4088, fax: 205-975-6522, Hyunki@uab.edu).

EMMPRIN antibody with/without cisplatin or radiation, the mean K^{trans} change for 3 days was significantly correlated with the mean tumor volume change for 7 days (r=0.74, *p*=0.0346), Ki67 expressing cell density (r=0.96, *p*=0.0001) and CD31 density (r=0.84, *p*=0.0084).

Conclusion—DCE-MRI might be utilized to assess the early therapeutic effects of anti-EMMPRIN antibody with/without chemotherapy or radiotherapy in head and neck cancer.

Keywords

DCE-MRI; head and neck cancer; anti-EMMPRIN antibody; cisplatin; radiotherapy

INTRODUCTION

Head and neck squamous cell carcinoma (HNSCC) is the most common type of head and neck cancer, accounting for about 3% of all cancers in the United States (1). Various chemotherapies, biological therapies, and radiotherapy (XRT) have been tested for HNSCC treatment in both adjuvant and neoadjuvant settings (2), with limited improvement in outcomes over the past several decades (3,4).

Molecular targeting of head and neck cancer has become a critical approach to improve results, but predicting the potential of these therapies has been difficult. Although, in some cases, the molecular biology of the tumor cell can predict response, this is the exception rather than the rule (5). As a result, non-invasive imaging modalities are being evaluated to predict patients likely to respond early in their therapy as a method of delivering personalized therapeutic cancer therapy (6–8). Dynamic contrast-enhanced magnetic resonance imaging (DCE-MRI) has been evaluated to assess early tumor response following chemotherapy (9–11) or XRT (12–14). DCE-MRI can retrieve pharmacokinetic parameters of an MR contrast agent in a target tissue monitoring the dynamic change of contrast concentration over time (15). Effective killing of cancer cells alters microvasculature in a tumor, represented by the change of K^{trans} (forward volume transfer constant: wash-in rate) values that are quantifiable from DCE-MR images (11,14). The early assessment of tumor response may improve clinical outcomes by discontinuing a failing treatment in a timely manner.

Extracellular matrix metalloprotease inducer (EMMPRIN) is a glycoprotein expressed on the plasma membrane of most cancer cells, and has been perceived as a good target for effective treatment of HNSCC (16). EMMPRIN promotes the production of matrix metalloproteinases (MMPs) by stimulating surrounding stromal cells as well as through an autocrine pathway (17–20). EMMPRIN also elevates neovascularization by stimulating endothelial cells to upregulate VEGFR-2 and promoting the production of VEGF isoforms (21). HNSCC expresses EMMPRIN at the highest level with dense fibrotic stroma (16,22). So the use of an antagonist targeting EMMPRIN is a promising approach to arrest tumor growth by suppressing both neovascularization and tissue invasion in HNSCC.

A monomeric monoclonal antibody targeting EMMPRIN, anti-EMMPRIN antibody, has demonstrated substantial anti-tumor effects in both HNSCC and pancreatic cancer mouse models (23–26). Anti-EMMPRIN therapy significantly decreased proliferating and

endothelial cells in tumors (23,24), and additive therapeutic effects were observed when additional chemotherapy or biological therapy was used in combination (25,26). The first line treatment for advanced HNSCC is cisplatin, a platinum-based chemotherapeutic agent, with concurrent X-radiation (27–29). We hypothesized that the combined use of anti-EMMPRIN antibody with cisplatin (or X-radiation) would improve the overall treatment effects in HNSCC. Anti-EMMPRIN antibody presented no adverse side effects in mice (30), thus it might be readily combined with conventional therapies in HNSCC.

The goal of this study was to evaluate DCE-MRI as a non-invasive tool for early therapy assessment of anti-EMMPRIN antibody when used in combination with cisplatin or X-radiation in HNSCC mouse models.

MATERIALS AND METHODS

Reagents and Cell lines

All reagents were from Fisher (Pittsburg, PA) unless otherwise specified. _____ provided purified monomeric monoclonal anti-EMMPRIN antibody (mouse origin IgG1 kappa). Cisplatin (Platinol®; Bristol-Myers Squibb, New York City, NY) and gadoteridol (Prohance®; Bracco Diagnostics Inc., Princeton, NJ) were purchased form the _____. Two human HNSCC cell lines derived from oral cavity (SCC1) and tong (OSC19) were obtained from _____, and cultured in Dulbecco's modified Eagle's medium (DMEM; Mediatech Inc, Herndon VA) supplemented with 10% fetal bovine serum (Hyclone, Logan, UT). EMMPRIN expressions in both the cell lines were confirmed by immunoblot analysis (data not shown).

Animal Preparation

Animal experiments were reviewed and approved by the Institutional Animal Care and Use Committee. A total of 12 groups of female athymic nude mice (4–6 weeks old) bearing subcutaneous human head and neck cancer xenografts were used. Table 1 presents the time schedule of dosing and imaging of all animals. Groups 1–6 were bearing SCC1 tumors, while groups 7–12 were bearing OSC19 tumors. Each animal was subcutaneously implanted with 2 million SCC1 (or OSC19) tumor cells. A total of 8 animals per group were originally employed, but 5 animals having similar tumor size (5–7 mm in diameter) and shape were selected per group at four weeks after cell implantation. A vascular access port (Access Technologies, Skokie, IL) was surgically implanted on the back of each animal to facilitate intravenous MR contrast injection as described in our previous study (31). Imaging and therapy were initiated at four days after port insertion. Groups 1–6 (or groups 7–12) were untreated (served as control) or treated with anti-EMMPRIN antibody (0.1 mg, days 0 and 3), X-radiation (2Gy, days 0 and 3), cisplatin (3mg/kg, day 0), anti-EMMPRIN antibody plus X-radiation, and anti-EMMPRIN antibody plus cisplatin, respectively. MRI was applied on days 0, 3, and 7. Five animals from groups 1, 8, 9, 11 and 12 (one animal from each group) were euthanized prior to completing studies due to ulceration on tumors, so those data were excluded. All the other animals were killed on day 7 after imaging, and tumors were collected for Ki67 and CD31 staining.

MRI

Small animal MRI was conducted with a Bruker BioSpec 9.4T system (Bruker BioSpin Corp., Billerica, MA). The tumor was imaged using a combination of a ^{1}H volume resonator/transmitter and a surface coil receiver (Bruker BioSpin Corp., Billerica, MA). A 27-gauge needle connected to a sterilized polyurethane tube (Strategic Applications Inc., Libertyville, IL) was inserted into the lumen of each port, to deliver gadoteridol. Anatomical MRI to measure tumor volume was performed using a relaxation enhancement (RARE) T2-weighted turbo spin-echo sequence with the following acquisition parameters: repetition time (TR)/echo time (TE) = 2000/34 milliseconds, 128×128 matrix, and a 30×30-mm field of view. Continuous 1-mm thick slices were used to cover the entire tumor region. T1 map was acquired with a gradient-echo multiflip-angle approach with the following parameters: repetition time (TR)/echo time (TE) = 115/3 milliseconds, 128×128 matrix, a 30×30-mm field of view, NEX=4, and seven flip angles of 10, 20, 30, 40, 50, 60, and 70°. A total of five to seven 1-mm thick slices were acquired to cover tumor regions of interest in an interlaced mode. DCE-MRI employed the same acquisition parameters as those above but with the fixed flip angle of 30°. Five baseline images were acquired before gadoteridol injection, and then 40 images were acquired after gadoteridol injection of 0.0267 mmol/ml over a period of 15 seconds with a total injection volume of 0.15 ml. A syringe pump (NE-1600, New Era Pump Systems, Inc., Wantagh, NY) was used to inject gadoteridol at a constant rate (0.01 ml/sec).

Image Analysis

The reference region (RR) model was employed to calculate K^{trans} values (32). RR model uses the signal enhancement in a reference region to remove the need for the arterial input function (AIF) as follows,

$$C_{t,ROI}(t)=(K^{trans,ROI}/K^{trans,RR})C_{t,RR}(t)+(K^{trans,ROI}/v_{e,RR})\int_0^t C_{t,RR}(t')dt'-(K^{trans,ROI}/v_{e,ROI})\int_0^t C_{t,ROI}(t')dt'$$

, where $C_{t,ROI}(t)$, $K^{trans,ROI}$, and $v_{e,ROI}$ are the contrast-agent concentration, volume transfer constant, and fractional extravascular-extracellular volume respectively in the tumor, while $C_{t,RR}(t)$, $K^{trans,RR}$, and $v_{e,RR}$ are those in the RR. 32 voxels (two 4×4 voxel windows) located in the perivertebral muscle were selected as the RR, and the $v_{e,RR}$ was assumed to be constant at 0.08 over the region (33). Tumor region was segmented in T2W MR images using a global thresholding technique in ImageJ, version 1.48 (National Institutes of Health, Bethesda, MD) (34). Then the iso-distance peripheral region with 0.5-mm thickness beginning from the tumor surface was segmented for each slice, while the random topological structure of the tumor was maintained as described in our previous study (31). The K^{trans} values averaged in the peripheral tumor region were reported in this manuscript unless otherwise specified. Segmentation of the whole tumor area was performed using ImageJ, version 1.48 (National Institutes of Health, Bethesda, MD). The K^{trans} quantification, peripheral tumor-region segmentation, and tumor-volume calculation were implemented using computer software developed using Labview, version 2010 (National Instruments Co., Austin, TX).

Histological Analysis

Ki67 and CD31 staining were implemented for all tumor tissues with the same procedure as reported (24). Three digital microphotographs (X200) were randomly taken for each tumor slice using SPOT camera on an Olympus 1×70 microscope (Olympus Optical Co., Tokyo, Japan), interfaced with personal computer and SPOT software. Ki67 expressing cells and CD31-stained area were segmented using a color thresholding technique. Ki67 expressing cell density (cell number/mm^2) and CD31 density (CD31-stained area/total area) were calculated per each photograph, and then averaged. The image analysis was performed using ImageJ, version 1.48 (National Institute of Heath, Bethesda, MD).

Statistical Analysis

One-way ANOVA was used to compare the changes of tumor volume (or K^{trans} values) among the groups that occurred during therapy (35). One-way ANOVA was also used to compare Ki67 expressing cell densities (or CD31 densities) in tumors. The Pearson correlation coefficient was used to look at the correlation between the mean K^{trans} changes and the mean tumor volume changes (or histological findings) (36). *p* values less than 0.05 were considered significant, after applying Bonferroni correction for multiple comparisons (35); when *p* value became bigger than 1 after Bonferroni correction, it was truncated to 1. 95% confidence intervals (CIs) were specified when non-significant *p* values were less than 0.2. Data are presented as means±standard error. All analyses were performed with SAS, version 9.4 (SAS Institute Inc., Cary, NC).

RESULTS

Figure 1 shows MR contrast maps of a representative SCC1 (or OSC19) tumor xenograft prior to therapy initiation at 2, 10 and 40 minutes after gadoteridol injection, together with the contrast enhancement curves in the region indicated with white rectangles in the contrast maps, and K^{trans} maps in the entire or 0.5-mm thick peripheral tumor region. The mean sizes of SCC1 and OSC19 tumors prior to therapy initiation were 145±32 mm^3 and 150±11 mm^3, respectively, without statistical difference (p=0.8816). The baseline K^{trans} values of SCC1 tumors prior to therapy initiation were 0.025±0.003 min^{-1} in the entire tumor region, and those in the peripheral tumor region were 0.027±0.003 min^{-1}. In OSC19 tumors, the baseline K^{trans} values in the entire and peripheral tumor regions were 0.035±0.002 min^{-1} and 0.034±0.003 min^{-1}, respectively. The baseline K^{trans} value averaged in the entire tumor region of SCC1 model was significantly lower than that of OSC19 model (p=0.0012), but those were not statistically different in the peripheral tumor region (p=0.0514; 95% CI: −0.0001, 0.0147).

Figures 2a and 2b show the changes of K^{trans} values averaged in the peripheral tumor region for a week of treatment in SCC1 and OSC19 models, respectively. The changes of K^{trans} values in SCC1 and OSC19 tumors treated with anti-EMMPRIN antibody for 3 days were −18±8% and 4±7%, respectively, which were significantly lower than those of control groups (39±5% and 45±7%; p=0.0025 and 0.0220, respectively). When cisplatin was used in combination, the K^{trans} changes for 3 days in SCC1 and OSC19 tumors were −42±9% and −44±9%, respectively, and those when combined with XRT were −45±9% and −27±10%,

respectively, which were also significantly lower than those of control groups (p<0.0001 for all four comparisons). After a week of anti-EMMPRIN monotherapy, the K^{trans} changes in SCC1 and OSC19 tumors were −25±10% and −6±6%, respectively, significantly lower than those of control groups (72±12% and 48±8%; p<0.0001 and 0.0010, respectively). When combined with cisplatin, those were −56±9% and −64±8%, respectively, and with XRT, −68±12% and −59±5%, respectively, significantly lower than those of control groups (p<0.0001 for all four comparisons). Interestingly, the mean K^{trans} value of SCC1 tumors treated with XRT increased 38±14% for 3 days after therapy initiation, and decreased thereafter. In the OSC19 model, however, XRT significantly reduced tumor K^{trans} values in 3 days after starting therapy as compared to control group (p=0.0004).

Figures 2c and 2d show the tumor volume changes during therapy in SCC1 and OSC19 models, respectively. Control tumor volume increased 23±9% and 84±21% in SCC1 model, and 66±7% and 171±9% in OSC19 model for 3 and 7 days, respectively. Anti-EMMPRIN monotherapy suppressed the tumor growth to 6±2% and 29±11% in SCC1 model, and 48±6% and 123±5% in OSC19 model, at 3 and 7 days after therapy initiation, respectively, but statistical difference from the control group was found only in OSC19 model on day 7 (p=0.0084). Anti-EMMPRIN antibody combined with cisplatin significantly suppressed tumor growth as compared to control group during both 3 and 7 days after therapy initiation in either SCC1 (−9±6% and −9±9%; p=0.0372 and 0.0005, respectively) or OSC19 model (26±4% and 76±7%; p=0.0002 and <0.0001, respectively). Similarly, combination therapy with XRT significantly suppressed tumor growth on both days 3 and 7 in SCC1 model (−25±6% and −34±19%; p=0.0005 and 0.0003, respectively), but only on day 7 in OSC19 model (43±5% and 91±12%; p=0.0672 (95% CI: −0.0093, 0.4691) and <0.0001, respectively).

Figures 3a and 4a show the microphotographs of representative tumors from the six groups in SCC1 and OSC19 models, respectively, following Ki67 and CD31 staining. Figures 3b and 4b represent Ki67 expressing cell densities in SCC1 and OSC19 tumors, respectively, while Figs. 3c and 4c represent CD31 densities. Mean Ki67 expressing cell densities of tumors treated with anti-EMMPRIN antibody were 60±18% and 37±8% lower than those of control tumors in SCC1 (p=0.1304; 95% CI: −67, 1019) and OSC19 (p=0.0214) models, respectively. In combination therapy with cisplatin, the mean Ki67 expressing cell densities were 83±4% and 75±3% lower than those of control tumors in SCC1 (p=0.0100) and OSC19 (p<0.0001) models, respectively, and with XRT, 85±1% and 68±3% lower than those of control tumors in SCC1 (p=0.0071) and OSC19 (p<0.0001) models, respectively. Mean CD31 densities of tumors treated with anti-EMMPRIN antibody were 71±11% and 44±3% lower than those of control tumors in SCC1 (p=0.0012) and OSC19 (p=0.0004) models, respectively. When anti-EMMPRIN antibody was used in combination with cisplatin, the mean CD31 densities were 77±8% and 51±8% lower than those of control tumors in SCC1 (p=0.0005) and OSC19 (p<0.0001) models, respectively, and with XRT, those were 77±7% and 78±6% lower than those of control tumors in SCC1 (p=0.0005) and OSC19 (p<0.0001) models, respectively.

Figure 5 shows the correlations between the mean tumor K^{trans} changes for 3 days (or 7 days) and the mean tumor volume change (or histological findings) of the twelve groups

bearing either SCC1 or OSC19 tumors. Since the mean K^{trans} value of SCC1 tumors was erroneously increased in 3 days after X-radiation monotherapy, data of the group were indicated with black diamonds, while the others were with gray circles. Without the data of SCC1 tumors treated with XRT, the mean tumor K^{trans} change for 3 days was significantly correlated with the mean tumor volume change for 7 days (p=0.0365), Ki67 expressing cell density (p=0.0003), or CD31 density (p=0.0027). When the data were included, however, the correlations were weakened; the mean tumor K^{trans} change for 3 days was not significantly correlated with the mean tumor volume change for 7 days (p=0.0628; 95% CI: −0.0320, 0.8550), but significantly correlated with the mean Ki67 expressing cell density (p=0.0064) or CD31 density (p=0.0122). Mean tumor K^{trans} change for 7 days was significantly correlated with all those above with or without XRT SCC1 tumor data. When only eight groups untreated (control) or treated with anti-EMMPRIN therapy with/without cisplatin or XRT were used, the mean tumor K^{trans} change for 3 days was significantly correlated with the mean tumor volume change for 7 days (r=0.7432, p=0.0346), Ki67 expressing cell density (r=0.9620, p=0.0001) or CD31 density (r=0.8442, p=0.0084), and the mean tumor K^{trans} change for 7 days was significantly correlated with the mean Ki67 expressing cell density (r=0.8967, p=0.0025) or CD31 density (r=0.7924, p=0.0190), but not with the mean tumor volume change for 7 days (r=0.6206, p=0.1006; 95% CI: −0.1494, 0.9221).

DISCUSSION

The early change of tumor K^{trans} values in the 0.5-mm peripheral tumor region after starting anti-EMMPRIN therapy with/without chemo- or radiotherapy was significantly correlated with the tumor-volume change for a week, proliferating (Ki67 expressing) cell density, or microvascular (CD31) density in human head and neck tumor xenografts. Central necrosis was often observed especially in SCC1 tumors, thus confining the region of interest (ROI) to the peripheral tumor region is a reasonable way to measure the therapeutic response of viable tumor tissues. Tumor K^{trans} changes, however, presented higher correlation with proliferating cell density or microvascular density, than with tumor volume change. This might be related to the presence of necrotic core in tumors. If a tumor develops necrotic core, tumor growth will be mainly determined by the cellular proliferation in the non-necrotic peripheral tumor tissue. Therefore, although a cancer drug induces the same magnitude of cytotoxicity in tumors, tumor growth may be the more rapidly arrested in tumors with the larger necrotic cores. So tumor K^{trans} change may represent the therapeutic efficacy of anti-EMMPRIN antibody with/without conventional treatments more accurately than tumor volume change.

Of interest, the K^{trans} values of SCC1 tumors treated with X-radiation monotherapy were increased for the first 3 days, whereas those of OSC19 tumors were not. Similarly, Janssen *et al* reported that the K^{trans} values in rectal tumors were significantly increased by radiotherapy in five days after therapy initiation (37), but Jakubovic *et al* reported that the K^{trans} values in brain metastases of responding patients were significantly reduced by a week of radiotherapy (38). This discrepancy might be explained by the difference in radiation susceptibility of endothelial cells in tumors. Presumably, if intratumoral endothelial cells susceptible to X-rays are preferentially killed by radiation, MR contrast

may leak out through the empty space on the vessel wall, which results in the rapid increase of wash-in rate (K^{trans}). Thereafter the vessels may be reassembled with X-ray resistant endothelial cells, leading to the reduction in K^{trans} value as well as microvessel density. When radiotherapy was combined with anti-EMMPRIN therapy, however, tumor K^{trans} value was significantly reduced in 3 days after therapy initiation even in SCC1 tumors; the intratumoral matrix might be more rapidly reassembled after more rapid killing of endothelial cells. If X-ray susceptibility of endothelial cells can be different across tumor types, the sudden increase of tumor K^{trans} values after X-radiation therapy during early therapeutic period might also represent the effectiveness of treatment. The variation in endothelia-cell susceptibility to X-radiation, however, may need to be further investigated.

The current study, however, has several limitations. First, tumor response was assessed for a relatively short time interval. Overall survival benefit will need to be examined in orthotopic and/or metastatic HNSCC tumor models in future studies, and then correlated with the early change of DCE-MRI pharmacokinetic parameters. We used subcutaneous tumor models, since mice bearing orthotopic oral tumor xenografts died before tumors grow to the proper size for a DCE-MRI based therapy study due to inability to eat. However, subcutaneous tumor model is not ideal to analyze tumor cell invasion and metastasis, which can be effectively suppressed by anti-EMMPRIN antibody. *In vivo* optical imaging of fluorophore labeled antibody targeting tumor cells will need to be employed to examine the progress of tumor boundary during anti-EMMPRIN therapy, as demonstrated in our previous study (39). Since cisplatin and X-radiation are often used in combination for HNSCC treatment (40), it would be also necessary to investigate whether the therapeutic efficacy of the chemoradiation can be improved when anti-EMMPRIN antibody is used concurrently.

In conclusion, the early change of tumor K^{trans} value in head and neck cancer mouse models was significantly correlated with tumor volume change, proliferating cell density, or microvessel density after anti-EMMPRIN antibody with/without chemotherapy or radiotherapy. Therefore quantitative DCE-MRI may be utilized as a non-invasive tool to assess the early tumor response following the novel therapies, which may lead to tailoring the therapeutic strategy to obtain the most favorable clinical outcomes in head and neck cancer patients. Prior to clinical translation, however, the toxicity of anti-EMMPRIN antibody with/without chemotherapy or radiation will need to be examined with non-human primates.

Acknowledgments

Grant support: NIH grants 2P30CA013148 and 5R01CA142637-03.

REFERENCES

1. Siegel R, Ma J, Zou Z, Jemal A. Cancer statistics, 2014. CA: a cancer journal for clinicians. 2014; 64:9–29. [PubMed: 24399786]
2. Brana I, Siu LL. Locally advanced head and neck squamous cell cancer: treatment choice based on risk factors and optimizing drug prescription. Ann Oncol. 2012; 23(Suppl 10):x178–x185. [PubMed: 22987958]
3. Rousseau A, Badoual C. Head and Neck: Squamous cell carcinoma: an overview. Atlas Genet Cytogenet Oncol Haematol. 2012; 16:145–155.

4. Casiglia J, Woo SB. A comprehensive review of oral cancer. Gen Dent. 2001; 49:72–82. [PubMed: 12004680]

5. Faratian D, Clyde RG, Crawford JW, Harrison DJ. Systems pathology--taking molecular pathology into a new dimension. Nat Rev Clin Oncol. 2009; 6:455–464. [PubMed: 19581910]

6. Eary JF, Conrad EU, O'Sullivan J, Hawkins DS, Schuetze SM, O'Sullivan F. Sarcoma mid-therapy [F-18]fluorodeoxyglucose positron emission tomography (FDG PET) and patient outcome. J Bone Joint Surg Am. 2014; 96:152–158. [PubMed: 24430415]

7. Williams TM, Galban S, Li F, Heist KA, Galban CJ, Lawrence TS, Holland EC, Thomae TL, Chenevert TL, Rehemtulla A, Ross BD. DW-MRI as a Predictive Biomarker of Radiosensitization of GBM through Targeted Inhibition of Checkpoint Kinases. Translational oncology. 2013; 6:133–142. [PubMed: 23544166]

8. Kim H, Keene KS, Sarver DB, Lee SK, Beasley TM, Morgan DE, Posey JA 3rd. Quantitative perfusion- and diffusion-weighted magnetic resonance imaging of gastrointestinal cancers treated with multikinase inhibitors: a pilot study. Gastrointest Cancer Res. 2014; 7:75–81. [PubMed: 25276260]

9. Cheung YC, Chen SC, Su MY, See LC, Hsueh S, Chang HK, Lin YC, Tsai CS. Monitoring the size and response of locally advanced breast cancers to neoadjuvant chemotherapy (weekly paclitaxel and epirubicin) with serial enhanced MRI. Breast Cancer Res Treat. 2003; 78:51–58. [PubMed: 12611457]

10. Martincich L, Montemurro F, De Rosa G, Marra V, Ponzone R, Cirillo S, Gatti M, Biglia N, Sarotto I, Sismondi P, Regge D, Aglietta M. Monitoring response to primary chemotherapy in breast cancer using dynamic contrast-enhanced magnetic resonance imaging. Breast Cancer Res Treat. 2004; 83:67–76. [PubMed: 14997056]

11. Jia Q, Xu J, Jiang W, Zheng M, Wei M, Chen J, Wang L, Huan Y. Dynamic contrast-enhanced MR imaging in a phase study on neoadjuvant chemotherapy combining Rh-endostatin with docetaxel and epirubicin for locally advanced breast cancer. Int J Med Sci. 2013; 10:110–118. [PubMed: 23329881]

12. Hoskin PJ, Saunders MI, Goodchild K, Powell ME, Taylor NJ, Baddeley H. Dynamic contrast enhanced magnetic resonance scanning as a predictor of response to accelerated radiotherapy for advanced head and neck cancer. The British journal of radiology. 1999; 72:1093–1098. [PubMed: 10700827]

13. Ceelen W, Smeets P, Backes W, Van Damme N, Boterberg T, Demetter P, Bouckenooghe I, De Visschere M, Peeters M, Pattyn P. Noninvasive monitoring of radiotherapy-induced microvascular changes using dynamic contrast enhanced magnetic resonance imaging (DCE-MRI) in a colorectal tumor model. International journal of radiation oncology, biology, physics. 2006; 64:1188–1196.

14. Ahn SJ, Koom WS, An CS, Lim JS, Lee SK, Suh JS, Song HT. Quantitative assessment of tumor responses after radiation therapy in a DLD-1 colon cancer mouse model using serial dynamic contrast-enhanced magnetic resonance imaging. Yonsei Med J. 2012; 53:1147–1153. [PubMed: 23074115]

15. Evelhoch JL, Gillies RJ, Karczmar GS, Koutcher JA, Maxwell RJ, Nalcioglu O, Raghunand N, Ronen SM, Ross BD, Swartz HM. Applications of magnetic resonance in model systems: cancer therapeutics. Neoplasia. 2000; 2:152–165. [PubMed: 10933074]

16. Riethdorf S, Reimers N, Assmann V, Kornfeld JW, Terracciano L, Sauter G, Pantel K. High incidence of EMMPRIN expression in human tumors. Int J Cancer. 2006; 119:1800–1810. [PubMed: 16721788]

17. Caudroy S, Polette M, Nawrocki-Raby B, Cao J, Toole BP, Zucker S, Birembaut P. EMMPRIN-mediated MMP regulation in tumor and endothelial cells. Clin Exp Metastasis. 2002; 19:697–702. [PubMed: 12553375]

18. Braundmeier AG, Fazleabas AT, Lessey BA, Guo H, Toole BP, Nowak RA. Extracellular matrix metalloproteinase inducer regulates metalloproteinases in human uterine endometrium. J Clin Endocrinol Metab. 2006; 91:2358–2365. [PubMed: 16522689]

19. Dalberg K, Eriksson E, Enberg U, Kjellman M, Backdahl M. Gelatinase A, membrane type 1 matrix metalloproteinase, and extracellular matrix metalloproteinase inducer mRNA expression: correlation with invasive growth of breast cancer. World J Surg. 2000; 24:334–340. [PubMed: 10658069]

20. Zucker S, Hymowitz M, Rollo EE, Mann R, Conner CE, Cao J, Foda HD, Tompkins DC, Toole BP. Tumorigenic potential of extracellular matrix metalloproteinase inducer. Am J Pathol. 2001; 158:1921–1928. [PubMed: 11395366]
21. Bougatef F, Quemener C, Kellouche S, Naimi B, Podgorniak MP, Millot G, Gabison EE, Calvo F, Dosquet C, Lebbe C, Menashi S, Mourah S. EMMPRIN promotes angiogenesis through hypoxia-inducible factor-2alpha-mediated regulation of soluble VEGF isoforms and their receptor VEGFR-2. Blood. 2009; 114:5547–5556. [PubMed: 19837976]
22. Liu Z, Hartman YE, Warram JM, Knowles JA, Sweeny L, Zhou T, Rosenthal EL. Fibroblast growth factor receptor mediates fibroblast-dependent growth in EMMPRIN-depleted head and neck cancer tumor cells. Mol Cancer Res. 2011; 9:1008–1017. [PubMed: 21665938]
23. Dean NR, Newman JR, Helman EE, Zhang W, Safavy S, Weeks DM, Cunningham M, Snyder LA, Tang Y, Yan L, McNally LR, Buchsbaum DJ, Rosenthal EL. Anti-EMMPRIN monoclonal antibody as a novel agent for therapy of head and neck cancer. Clin Cancer Res. 2009; 15:4058–4065. [PubMed: 19509148]
24. Kim H, Zhai G, Liu Z, Samuel S, Shah N, Helman EE, Knowles JA, Stockard CR, Fineberg NS, Grizzle WE, Zhou T, Zinn KR, Rosenthal EL. Extracelluar matrix metalloproteinase as a novel target for pancreatic cancer therapy. Anti-cancer drugs. 2011; 22:864–874. [PubMed: 21730821]
25. Kim H, Zhai G, Samuel SL, Rigell CJ, Umphrey HR, Rana S, Stockard CR, Fineberg NS, Zinn KR. Dual combination therapy targeting DR5 and EMMPRIN in pancreatic adenocarcinoma. Molecular cancer therapeutics. 2012; 11:405–415. [PubMed: 22203731]
26. Shah N, Zhai G, Knowles JA, Stockard CR, Grizzle WE, Fineberg N, Zhou T, Zinn KR, Rosenthal EL, Kim H. (18)F-FDG PET/CT imaging detects therapy efficacy of anti-EMMPRIN antibody and gemcitabine in orthotopic pancreatic tumor xenografts. Molecular imaging and biology : MIB : the official publication of the Academy of Molecular Imaging. 2012; 14:237–244. [PubMed: 21494920]
27. Forastiere AA, Goepfert H, Maor M, Pajak TF, Weber R, Morrison W, Glisson B, Trotti A, Ridge JA, Chao C, Peters G, Lee DJ, Leaf A, Ensley J, Cooper J. Concurrent chemotherapy and radiotherapy for organ preservation in advanced laryngeal cancer. The New England journal of medicine. 2003; 349:2091–2098. [PubMed: 14645636]
28. Adelstein DJ, Li Y, Adams GL, Wagner H Jr, Kish JA, Ensley JF, Schuller DE, Forastiere AA. An intergroup phase III comparison of standard radiation therapy and two schedules of concurrent chemoradiotherapy in patients with unresectable squamous cell head and neck cancer. Journal of clinical oncology : official journal of the American Society of Clinical Oncology. 2003; 21:92–98. [PubMed: 12506176]
29. Bachaud JM, Cohen-Jonathan E, Alzieu C, David JM, Serrano E, Daly-Schveitzer N. Combined postoperative radiotherapy and weekly cisplatin infusion for locally advanced head and neck carcinoma: final report of a randomized trial. International journal of radiation oncology, biology, physics. 1996; 36:999–1004.
30. Kim H, Rigell CJ, Zhai G, Lee SK, Samuel SL, Martin A, Umphrey HR, Stockard CR, Beasley TM, Buchsbaum DJ, Li LS, Boothman DA, Zinn KR. Antagonistic effects of anti-EMMPRIN antibody when combined with chemotherapy against hypovascular pancreatic cancers. Molecular imaging and biology : MIB : the official publication of the Academy of Molecular Imaging. 2014; 16:85–94. [PubMed: 23836505]
31. Kim H, Folks KD, Guo L, Stockard CR, Fineberg NS, Grizzle WE, George JF, Buchsbaum DJ, Morgan DE, Zinn KR. DCE-MRI detects early vascular response in breast tumor xenografts following anti-DR5 therapy. Molecular imaging and biology : MIB : the official publication of the Academy of Molecular Imaging. 2011; 13:94–103. [PubMed: 20383593]
32. Yankeelov TE, Luci JJ, Lepage M, Li R, Debusk L, Lin PC, Price RR, Gore JC. Quantitative pharmacokinetic analysis of DCE-MRI data without an arterial input function: a reference region model. Magn Reson Imaging. 2005; 23:519–529. [PubMed: 15919597]
33. Yankeelov TE, Cron GO, Addison CL, Wallace JC, Wilkins RC, Pappas BA, Santyr GE, Gore JC. Comparison of a reference region model with direct measurement of an AIF in the analysis of DCE-MRI data. Magn Reson Med. 2007; 57:353–361. [PubMed: 17260371]

34. Sarkar S, Das S. Multilevel image thresholding based on 2D histogram and maximum Tsallis entropy--a differential evolution approach. IEEE Trans Image Process. 2013; 22:4788–4797. [PubMed: 23955760]

35. Neter, J.; Kutner, MH.; Nachtsheim, JC.; Wasserman, W. Applied linear statistical models. Columbus: The McGraw-Hill Companies, Inc.; 1996.

36. Rodgers JL, Nicewander WA. Thirteen ways to look at the correlation coefficient. The American Statistician. 1988; 42:59–66.

37. Janssen MH, Aerts HJ, Kierkels RG, Backes WH, Ollers MC, Buijsen J, Lambin P, Lammering G. Tumor perfusion increases during hypofractionated short-course radiotherapy in rectal cancer: sequential perfusion-CT findings. Radiother Oncol. 2010; 94:156–160. [PubMed: 20080311]

38. Jakubovic R, Sahgal A, Soliman H, Milwid R, Zhang L, Eilaghi A, Aviv RI. Magnetic Resonance Imaging-based Tumour Perfusion Parameters are Biomarkers Predicting Response after Radiation to Brain Metastases. Clin Oncol (R Coll Radiol). 2014; 26:704–712. [PubMed: 25023291]

39. Heath CH, Deep NL, Sweeny L, Zinn KR, Rosenthal EL. Use of panitumumab-IRDye800 to image microscopic head and neck cancer in an orthotopic surgical model. Annals of surgical oncology. 2012; 19:3879–3887. [PubMed: 22669455]

40. Paul S, Chaudhuri T, Pant MC, Parmar D, Srivastava K. Association of cytochrome P450 2C9 polymorphism with locally advanced head and neck squamous cell carcinoma and response to concurrent cisplatin-based radical chemoradiation. South Asian J Cancer. 2014; 3:154–158. [PubMed: 25136521]

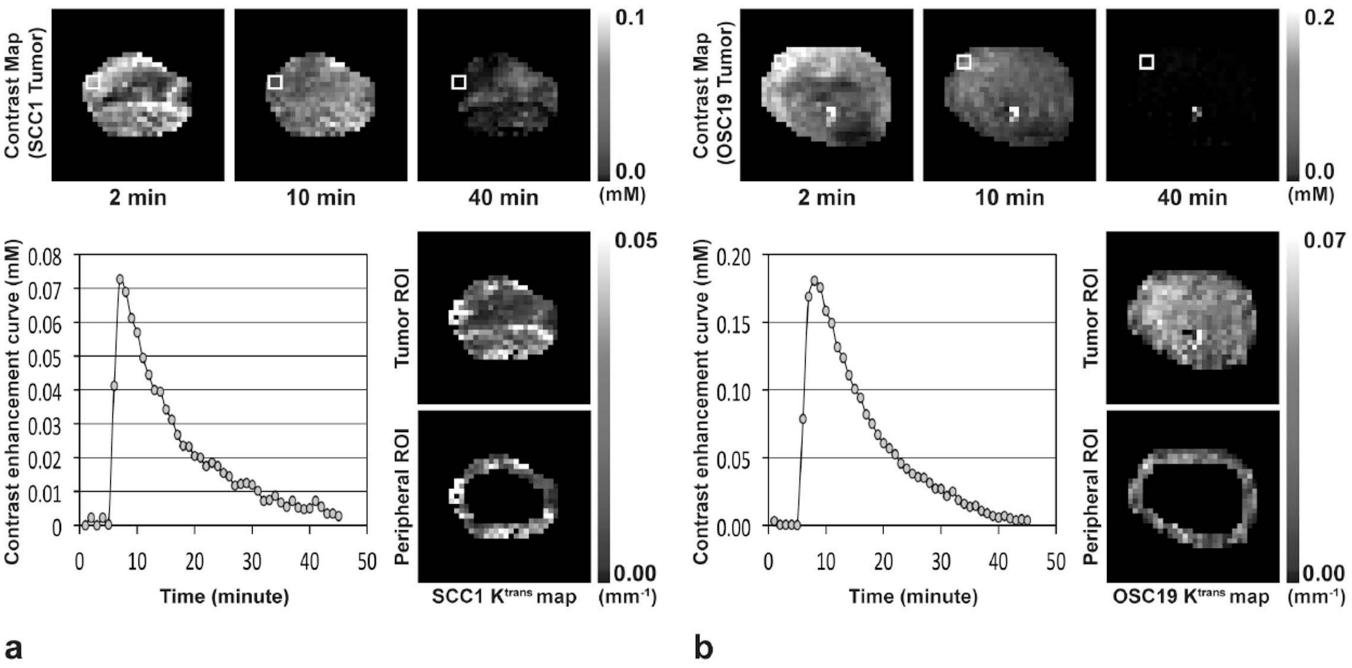

Figure 1.

MR contrast maps at 2, 10, and 40 minutes after gadoteridol injection, and K^{trans} maps in entire tumor region or 0.5-mm thick peripheral tumor region of representative (a) SCC1 and (b) OSC19 tumors prior to therapy initiation. Contrast enhancement curves averaged in the four pixels indicated with solid white box in each contrast map are shown.

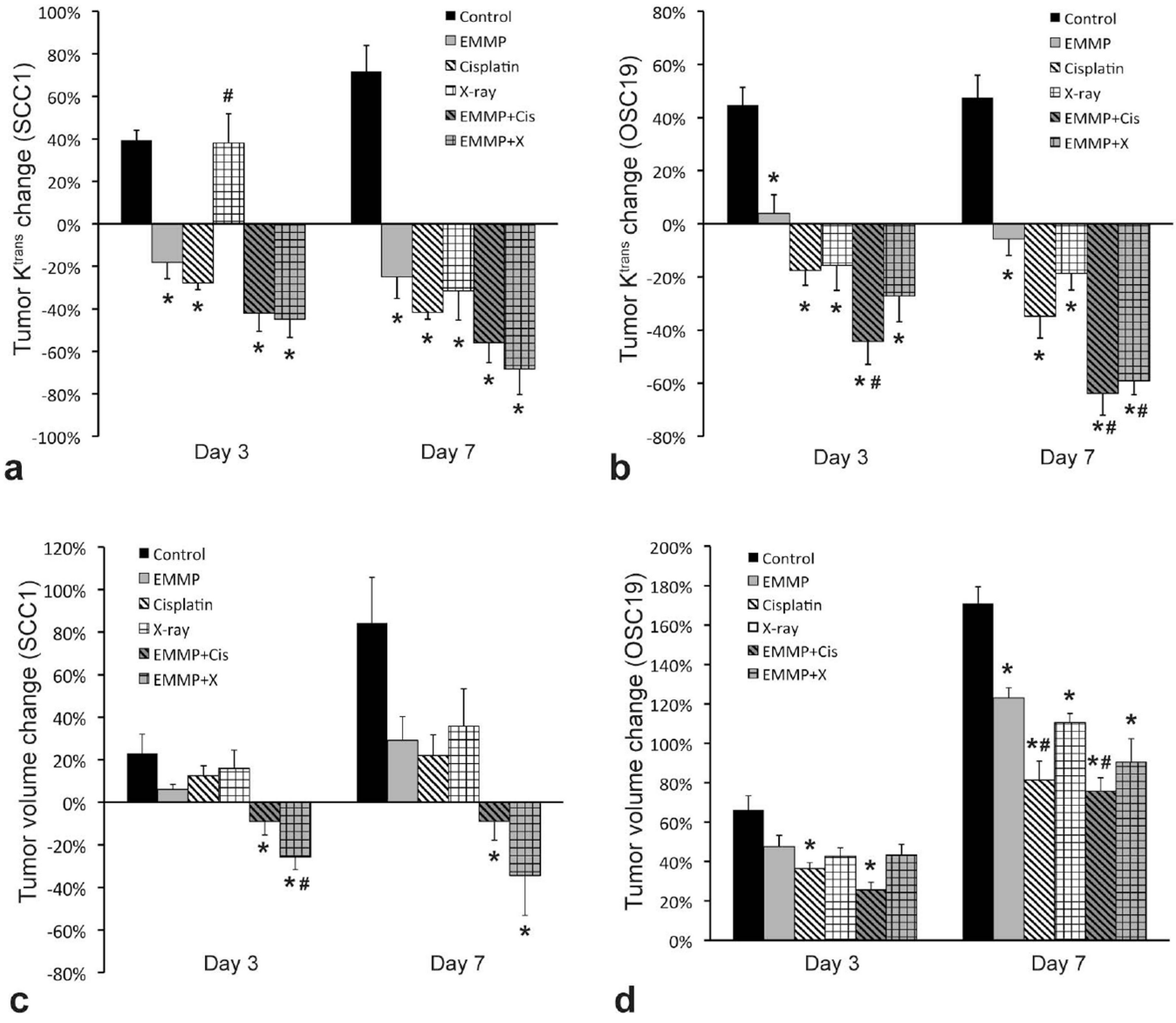

Figure 2.

K^{trans} change in 0.5-mm thick peripheral tumor region and tumor volume change in two human head and neck cancer mouse models. (a, b) K^{trans} change in 0.5-mm thick peripheral region of (a) SCC1 and (b) OSC19 tumors for 3 and 7 days after therapy initiation. (c, d) Volume change of (c) SCC1 and (d) OSC19 tumors for 3 and 7 days after therapy initiation. Six groups of animals (n=4–5 per group) were untreated (served as control) or treated with anti-EMMPRIN antibody (EMMP), cisplatin, X-ray irradiation, anti-EMMPRIN antibody plus cisplatin (EMMP+Cis), and anti-EMMPRIN antibody plus X-ray irradiation (EMMP +X), respectively. Asterisk and hash mark represent statistical difference from control and anti-EMMPRIN treated groups, respectively.

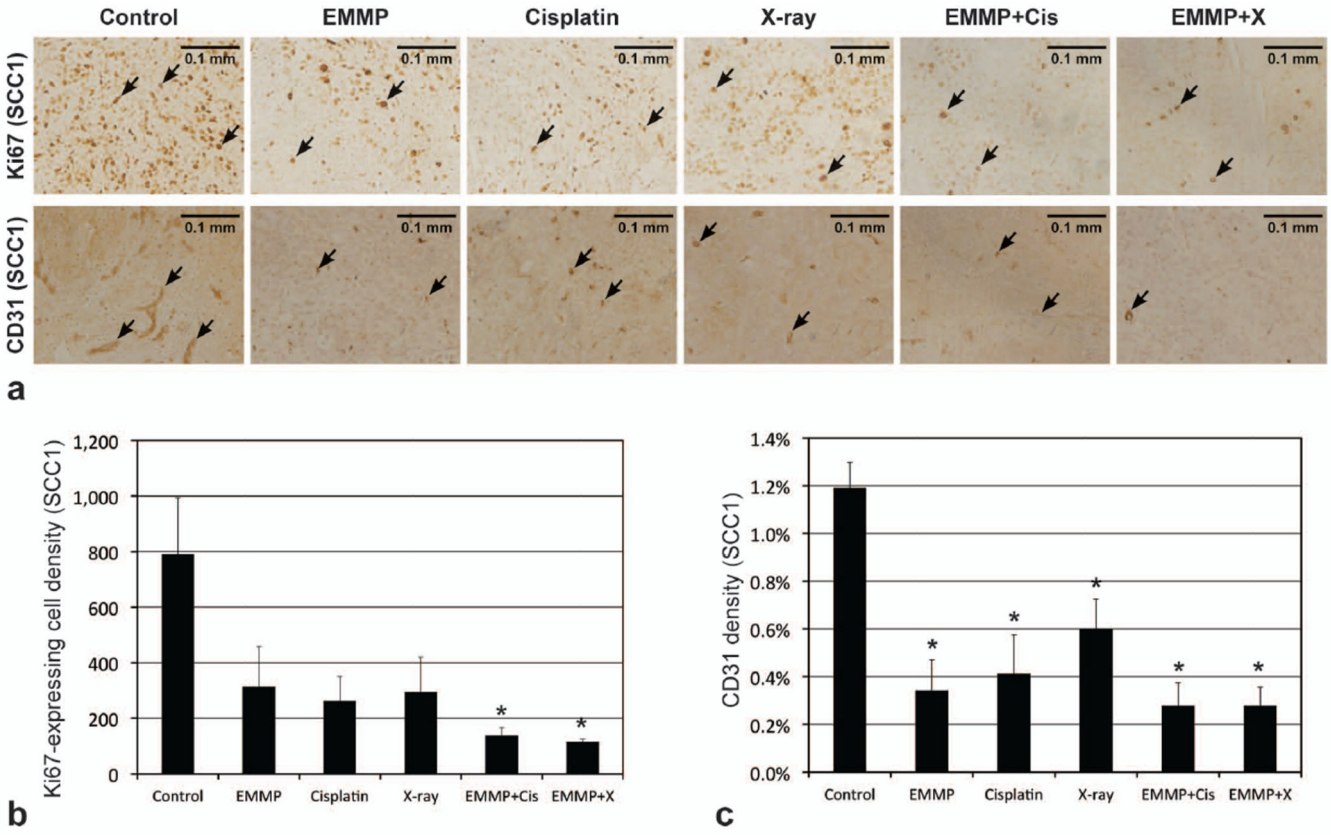

Figure 3.

Histological analyses of SCC1 tumors. (a) Representative microphotographs of Ki67 and CD31 stained tumor slices (5 μm thickness), when tumors were untreated (control) or treated with anti-EMMPRIN antibody (EMMP), cisplatin, X-ray irradiation, anti-EMMPRIN antibody plus cisplatin (EMMP+Cis), and anti-EMMPRIN antibody plus X-ray irradiation (EMMP+X), respectively. Ki67 expressing (proliferating) and CD31 stained (endothelial) cells are indicated with black arrows, and the length of each scale bar is 0.1 mm. (b) Ki67 expressing cell and (c) CD31 densities (mean±SE). Asterisk represents statistical difference from control group.

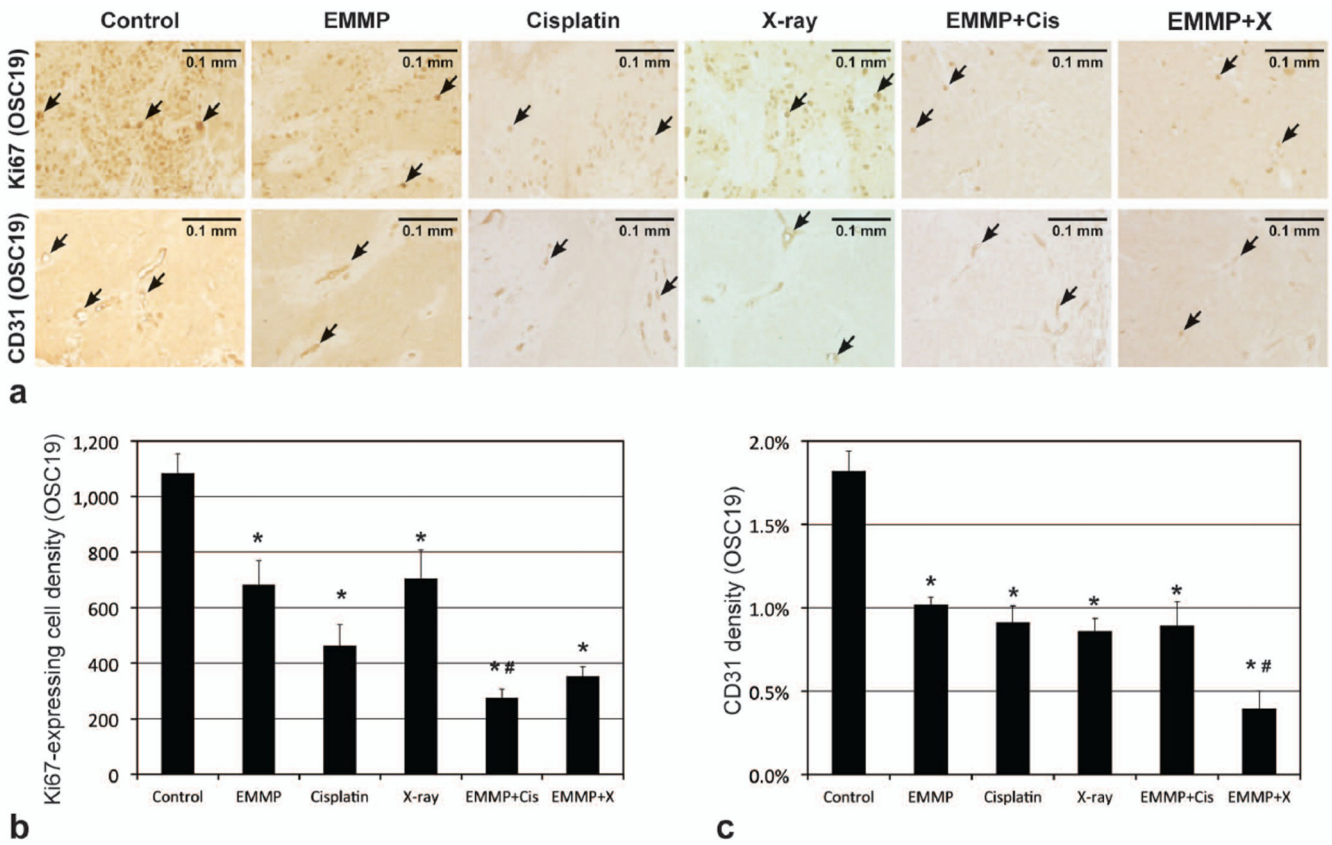

Figure 4.

Histological analyses of OSC19 tumors. (a) Representative microphotographs of Ki67 and CD31 stained tumor slices (5 μm thickness), when tumors were untreated (control) or treated with anti-EMMPRIN antibody (EMMP), cisplatin, X-ray irradiation, anti-EMMPRIN antibody plus cisplatin (EMMP+Cis), and anti-EMMPRIN antibody plus X-ray irradiation (EMMP+X), respectively. Ki67 expressing (proliferating) and CD31 stained (endothelial) cells are indicated with black arrows, and the length of each scale bar is 0.1 mm. (b) Ki67 expressing cell and (c) CD31 densities (mean±SE). Asterisk and hash mark represent statistical difference from control and anti-EMMPRIN treated groups, respectively.

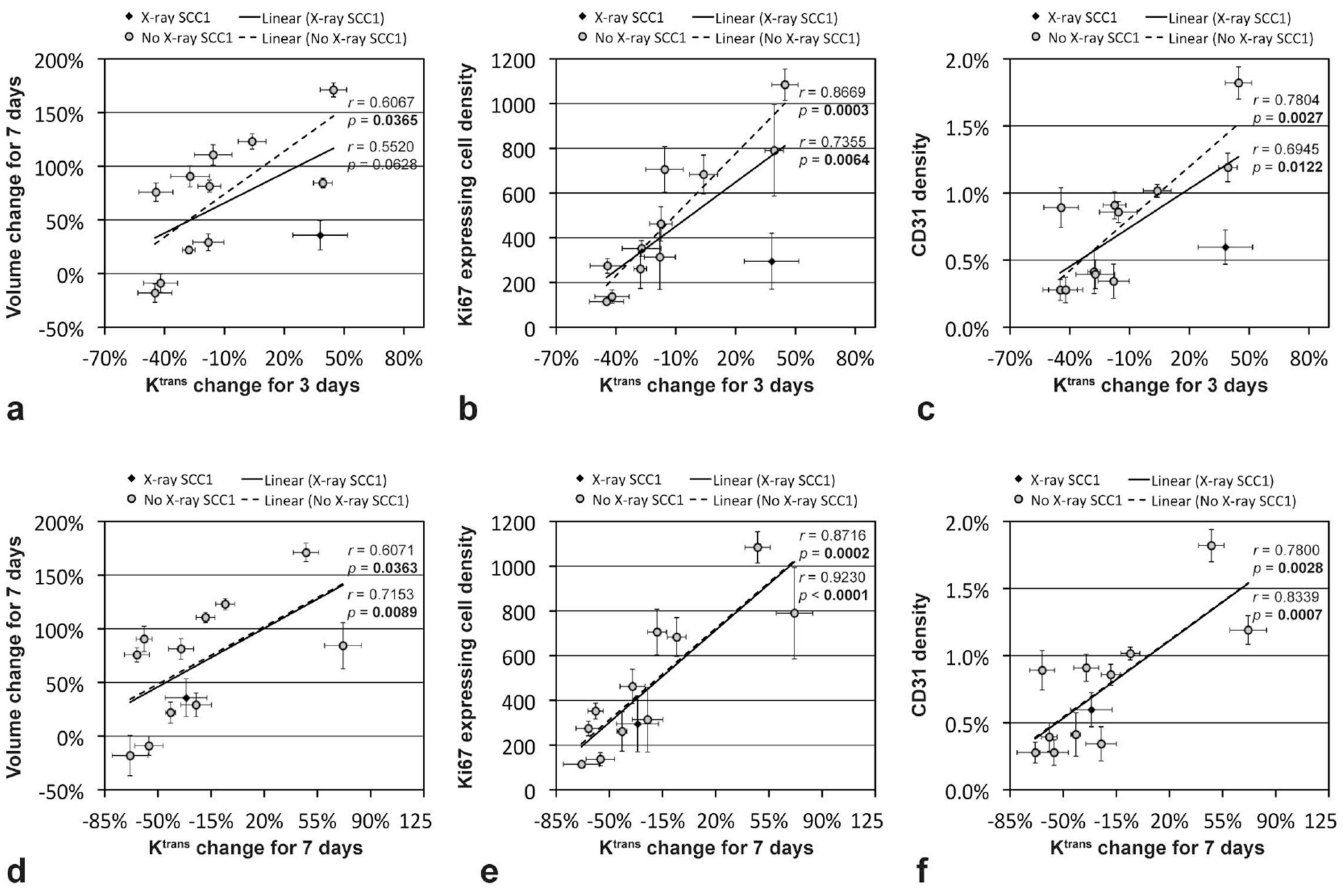

Figure 5.

Correlation between the mean tumor K^{trans} change (either for 3 days or 7 days) and the mean tumor volume change for 7 days (or histological findings). A total of 12 groups (6 groups per each tumor type) were untreated (served as control) or treated with anti-EMMPRIN antibody, cisplatin, X-ray irradiation, anti-EMMPRIN antibody plus cisplatin, and anti-EMMPRIN antibody plus X-ray irradiation. Data of SCC1 tumors treated with X-radiation monotherapy were indicated with black diamonds, while the others were with gray circles. Pearson correlation coefficients and p values were found when X-ray treated SCC1 data were included (listed above) or excluded (listed below).

Table 1

Time schedule of drug (or X-radiation) dosing and imaging of animals.

Tumor type	Groups	Time (days) after therapy initiation		
		Day 0	Day 3	Day 7
SCC1	Group 1 (n=4)	DCE-MRI	DCE-MRI	DCE-MRI
	Group 2 (n=5)	Anti-EMMPRIN Ab (0.1 mg) DCE-MRI before dosing	Anti-EMMPRIN Ab (0.1 mg) DCE-MRI before dosing	DCE-MRI
	Group 3 (n=5)	Cisplatin (3 mg/kg) DCE-MRI before dosing	Cisplatin (3 mg/kg) DCE-MRI before dosing	DCE-MRI
	Group 4 (n=5)	X-radiation (2Gy) DCE-MRI before dosing	X-radiation (2Gy) DCE-MRI before dosing	DCE-MRI
	Group 5 (n=5)	Anti-EMMPRIN Ab (0.1 mg) cisplatin (3 mg/kg) DCE-MRI before dosing	Anti-EMMPRIN Ab (0.1 mg) cisplatin (3 mg/kg) DCE-MRI before dosing	DCE-MRI
	Group 6 (n=5)	Anti-EMMPRIN Ab (0.1 mg) X-radiation (2Gy) DCE-MRI before dosing	Anti-EMMPRIN Ab (0.1 mg) X-radiation (2Gy) DCE-MRI before dosing	DCE-MRI
OSC19	Group 7 (n=5)	DCE-MRI	DCE-MRI	DCE-MRI
	Group 8 (n=4)	Anti-EMMPRIN Ab (0.1 mg) DCE-MRI before dosing	Anti-EMMPRIN Ab (0.1 mg) DCE-MRI before dosing	DCE-MRI
	Group 9 (n=4)	Cisplatin (3 mg/kg) DCE-MRI before dosing	Cisplatin (3 mg/kg) DCE-MRI before dosing	DCE-MRI
	Group 10 (n=5)	X-radiation (2Gy) DCE-MRI before dosing	X-radiation (2Gy) DCE-MRI before dosing	DCE-MRI
	Group 11 (n=4)	Anti-EMMPRIN Ab (0.1 mg) cisplatin (3 mg/kg) DCE-MRI before dosing	Anti-EMMPRIN Ab (0.1 mg) cisplatin (3 mg/kg) DCE-MRI before dosing	DCE-MRI
	Group 12 (n=4)	Anti-EMMPRIN Ab (0.1 mg) X-radiation (2Gy) DCE-MRI before dosing	Anti-EMMPRIN Ab (0.1 mg) X-radiation (2Gy) DCE-MRI before dosing	DCE-MRI